

The Decoupled Direct Method for Sensitivity Analysis in a Three-Dimensional Air Quality Model — Implementation, Accuracy, and Efficiency

ALAN M. DUNKER,*† GREG YARWOOD,‡
JEROME P. ORTMANN,† AND
GARY M. WILSON‡

*Chemical and Environmental Sciences Laboratory,
General Motors Research and Development Center,
Warren, Michigan 48090-9055, and ENVIRON International
Corp., Novato, California 94945-5010*

The decoupled direct method (DDM) has been implemented in a three-dimensional (3D) air quality model in order to calculate first-order sensitivities with respect to emissions and initial and boundary concentrations. This required deriving new equations for the sensitivities from the equations of the hybrid chemistry solver and the nonlinear advection algorithm in the model. The sensitivities for the chemistry and advection steps were tested in box-model and rotating-hill simulations, respectively. The complete model was then applied to an ozone episode of the Lake Michigan region during July 7–13, 1995. The DDM was found to be highly accurate for calculating the sensitivity of the 3D model. The sensitivities obtained by perturbing the inputs (brute-force method) converged toward the DDM sensitivities, as the brute-force perturbations became small. Ozone changes predicted with the DDM sensitivities were also compared to actual changes obtained from simulations with reduced inputs. For 40% reductions in volatile organic compound and/or NO_x emissions, the predicted changes correlate highly with the actual changes and are directionally correct for nearly all grid cells in the modeling domain. However, the magnitude of the predicted changes is 10–20% smaller than the actual changes on average. Agreement between predicted and actual ozone changes is better for 40% reductions in initial or boundary concentrations. Calculating one sensitivity by the DDM is up to 2.5 times faster than calculating the concentrations alone.

Introduction

Sensitivity coefficients measure how the concentrations predicted by an air quality model depend on input data and model parameters. As such, they have a variety of uses. They can provide directional, semiquantitative, or quantitative estimates of the effects of emission changes (1, 2). When combined with estimates of uncertainties in model inputs, sensitivities provide estimates of uncertainties in the predicted concentrations (3). An incremental reactivity factor is

the sensitivity of the ozone concentration to emissions of individual volatile organic compounds (VOCs) (4, 5). Sensitivities can be used to estimate rate constants from experimental measurements (6) or emission inventories from ambient measurements (7). Further, sensitivities can be used to develop a simplified representation of a model over a specific range of input variables and parameters (8).

First-order sensitivities describe the linear response of the model to a change in input parameters, and higher-order sensitivities describe the quadratic, cubic, and higher power responses. Because the number of higher-order sensitivities increases rapidly with the power of the response it is generally practical to calculate only the first-order sensitivities, though second-order sensitivities have sometimes been determined (8, 9). The major limitation of first-order sensitivities is that these describe the model response over a limited range of the input parameters. However, first-order sensitivities are still valuable for improving the efficiency of a global sensitivity analysis by selecting the parameters for study (10) or guiding the Monte Carlo algorithm (11). Furthermore, the results of global sensitivity analyses have often shown that the model response to parameter changes is relatively linear (e.g., the Monte Carlo samples are analyzed by linear regression) (10, 11).

Varying the input parameters one by one in separate model simulations and evaluating the change in predicted concentrations is the simplest approach to obtaining sensitivities (usually termed the brute-force method [BFM]). More sophisticated methods have been developed and applied to air quality models in an attempt to improve the accuracy, efficiency, and/or convenience of calculating sensitivities. The major approaches are the decoupled direct method (DDM) (12, 13), the Green's function method (9, 14), automatic differentiation in FORTRAN (ADIFOR) (15–17), and the adjoint method (18). A variation of the DDM, called DDM-3D, has also been developed recently (19). Of these methods, it appears that the DDM, DDM-3D, and adjoint methods have been applied to three-dimensional (3D) air quality models.

The DDM was originally developed for a first-generation model of ozone formation (12). This paper describes a new implementation of the method for a current model, the Comprehensive Air Quality Model with extensions (CAMx) (20, 21). Our focus is on obtaining first-order sensitivities with respect to initial concentrations, boundary concentrations, and emissions. However, one can also obtain sensitivities with respect to any other input parameters using the DDM. We provide substantial flexibility in defining the sensitivities, e.g., we allow sensitivities to different input chemical species and to variations in the spatial and temporal form of the inputs. We give details of the implementation for the chemistry and advection algorithms because these require the key, new additions to CAMx. Results of separate, stand-alone tests for these algorithms are presented next. We also applied the complete model to an ozone episode in the Lake Michigan region on July 7–13, 1995. The accuracy of the DDM sensitivities in this application is investigated by comparison to results from the BFM. In addition, we examine how well the first-order sensitivities describe the model response to different input perturbations.

The CAMx with the DDM is publicly available (22). CAMx also includes a technique for apportioning ozone concentrations to emissions and initial and boundary concentrations of VOC and NO_x. In a related paper (23), we compare these ozone source contributions with the corresponding ozone sensitivities obtained by the DDM.

* Corresponding author phone: (586)986-1625; fax: (586)986-1910; e-mail: alan.m.dunker@gm.com.

† General Motors Research and Development Center.

‡ ENVIRON International Corp.

Methodology

Air Quality Model. The CAMx is an Eulerian photochemical model for urban and regional simulations of ozone formation in the lower troposphere. It can accommodate multiple, nested, 3D grids with two-way communication between the coarser and finer grids. The model simulates the emission, advection, dispersion, chemical reactions, and removal of pollutants. There are various choices for the advection solver, the chemistry solver, and the chemical mechanism. In our work, we used the Bott algorithm (24) for advection and the hybrid solver for the chemistry (21). Most simulations were done with the Carbon Bond IV (CB IV) mechanism (25) with updated radical termination and isoprene reactions (26), but some tests of the chemistry solver used the Statewide Air Pollution Research Center 1997 (SAPRC97) mechanism (27). Dry deposition is represented in CAMx by the resistance model of Wesely (28), and wet deposition is represented by a simple scavenging model (29). Additional details and capabilities of CAMx are given elsewhere (21).

Overview of the DDM. We implemented the DDM by first defining

$$I(x,y,z,t,\lambda) = I_0(x,y,z,t) + \lambda \cdot g(x,y,z,t) \quad (1)$$

Here, I_0 is one of the model inputs (emissions, initial or boundary concentrations) for the base case, λ is a parameter, g is a function describing the change of interest, and I is the new input for the model. We calculate the sensitivity to λ , which represents the sensitivity to altering the model input from I_0 toward I . The form of eq 1 is quite flexible because g can have a different spatial (x, y, z) and temporal (t) dependence than I_0 . E.g., g could represent the emissions from a new source with a different geographic and diurnal dependence than other emissions. If $g = I_0$, however, λ simply scales the input by a constant factor. The input chemical species can be studied singly (a separate parameter λ_i for each species) or in groups (one parameter for all VOC or NO_x species).

If $\underline{\lambda}$ is the array of m parameters being considered and c_p is the concentration of any species p in the model output, then the q th order sensitivity coefficient is the q th order derivative in the Taylor series expansion:

$$c_p(x,y,z,t,\underline{\lambda}) = c_p(x,y,z,t,\underline{\lambda} = 0) + \sum_{i=1}^m \frac{\partial c_p}{\partial \lambda_i} \Big|_{\underline{\lambda}=0} \lambda_i + \frac{1}{2} \sum_{i=1}^m \sum_{j=1}^m \frac{\partial^2 c_p}{\partial \lambda_i \partial \lambda_j} \Big|_{\underline{\lambda}=0} \lambda_i \lambda_j + \dots \quad (2)$$

Note that this is an expansion about the base case, $\underline{\lambda} = 0$, and that these are absolute, not seminormalized (19), sensitivities. Because the λ_i are dimensionless, the sensitivities have the units of concentration. Furthermore, if all the $\lambda_i = 1$, the second term on the right-hand side in eq 2 is just the sum of the first-order sensitivities. Hence, a first-order sensitivity itself represents the (first-order) effect of an increase in λ_i from 0 to 1. Finally, in the special case $g = I_0$ in eq 1, a first-order sensitivity represents the effect of a 100% increase in I_0 .

In simplified form, the governing equation of the model is

$$\frac{\partial c_p}{\partial t} = \text{advection} + \text{diffusion} + \text{chemistry} + \text{emissions} + \text{deposition} \quad (3)$$

(The detailed terms for each process on the right-hand side are given elsewhere (21).) By introducing a 3D spatial grid x_i, y_j, z_k , a sequence of times t_k , and a numerical algorithm for each process, we obtain an approximation to eq 3:

$$\left[\frac{\Delta C_p}{\Delta t} \right]_{i,j,k,l} = \frac{\overline{\text{advection}} + \overline{\text{diffusion}} + \overline{\text{chemistry}} + \overline{\text{emissions}} + \overline{\text{deposition}}}{\text{emissions} + \text{deposition}} \Big|_{i,j,k,l} \quad (4)$$

In eq 4, C_p is the numerical approximation to c_p , $\overline{\text{process}}$ is the representation of the process by the numerical algorithm, and the subscripts i, j, k, l indicate that the terms are evaluated using concentrations on the chosen space-time grid.

To obtain the first-order sensitivity to λ in eq 1 by the DDM, we differentiate eq 4 with respect to λ :

$$\left[\frac{\Delta S_p}{\Delta t} \right]_{i,j,k,l} = \left[\frac{\partial \overline{\text{advection}}}{\partial \lambda} + \frac{\partial \overline{\text{diffusion}}}{\partial \lambda} + \frac{\partial \overline{\text{chemistry}}}{\partial \lambda} + \frac{\partial \overline{\text{emissions}}}{\partial \lambda} + \frac{\partial \overline{\text{deposition}}}{\partial \lambda} \right]_{i,j,k,l} \quad (5)$$

Here, $S_p = \partial C_p / \partial \lambda$ is the sensitivity of the numerical solution C_p , and $\partial \overline{\text{process}} / \partial \lambda$ denotes differentiation of the numerical algorithm for the process. (The initial and boundary conditions for eq 5 are obtained by differentiating the initial and boundary concentrations for eq 4 with respect to λ .) An important feature of the DDM is that the *same* spatial grid, time steps, and algorithms are used to calculate the sensitivities as are used to calculate the concentrations. This ensures maximum consistency between the sensitivities and the concentrations and between sensitivities obtained by the DDM and by the BFM. There are also other important advantages of the DDM discussed elsewhere (12).

The reason for choosing the same time steps is illustrated by the chemistry equations. Equations 4 and 5 are solved by a time-splitting algorithm, i.e., the full equation is broken into separate equations for each process, which are solved sequentially. Before introducing the time steps, the equations for the chemistry step are

$$\frac{dC}{dt} = f(C,t) \quad (6)$$

$$\frac{dS}{dt} = JS \quad (7)$$

C and S are vectors of the concentrations and sensitivities, respectively, of all species in a grid cell, f is a vector of reaction rates, and J is the Jacobian matrix $J_{ij} = \partial f_i / \partial C_j$. The time steps required to solve these equations are determined primarily by their stiffness, which in turn is determined by the Jacobian matrix (30). Since both equations have the same Jacobian, the same time steps will generally be required to solve eqs 6 and 7 to the same accuracy with a particular algorithm. A major difference between the DDM and the DDM-3D (19) is that the DDM-3D employs different algorithms and time steps for eqs 6 and 7. This complicates the error control and can lead to inconsistencies between the sensitivities and concentrations.

Implementing the DDM in any model requires locating those steps where a nonlinear response may arise, because in such steps the equations for the sensitivities have a different form than the equations for the concentrations. For CAMx, we made required changes for a nonlinear process (chemistry), a nonlinear algorithm (Bott algorithm for horizontal advection), and nonlinear bounds on the concentrations. Each of these changes is described below. No changes are required for other steps in the model, where the governing equation and algorithm are both linear and thus the equations for propagating the concentrations and sensitivities are identical. In such steps, however, it is often possible to improve efficiency by appropriately combining calculation

of concentrations and sensitivities, and we made some such optional changes for diffusion, vertical advection, and deposition.

Chemistry Step. The chemistry equations are themselves nonlinear, and hence the equations to propagate the sensitivities (eq 7) are different from the equations to propagate the concentrations (eq 6). The hybrid solver, which was developed specifically for CAMx, divides the chemical species into three groups: radicals, fast species (rapidly changing in time), and slow species. The CB IV mechanism has 12 radicals, 4 fast species, and 21 slow species, and the SAPRC97 mechanism has 33 radicals, 8 fast species, and 32 slow species. Radicals are represented by implicit, steady-state equations. For the fast and slow species, the semiimplicit, Crank-Nicolson algorithm and the explicit, Euler algorithm are employed, respectively. Thus,

$$f_R(\underline{C}_0^R, \underline{C}_0^F, \underline{C}_0^S) = 0 \quad \text{radicals} \quad (8)$$

$$\underline{C}_1^F = \underline{C}_0^F + \Delta t \cdot f_F(\underline{C}_0^R, \underline{C}_0^F, \underline{C}_0^S) \quad \text{fast species} \quad (9)$$

$$\underline{C}_1^S = \underline{C}_0^S + \Delta t \cdot f_S(\underline{C}_0^R, \underline{C}_0^F, \underline{C}_0^S) \quad \text{slow species} \quad (10)$$

where the superscripts *R*, *F*, and *S* indicate radicals, fast, and slow species, respectively, the subscripts indicate the beginning (t_0) and new (t_1) times, $\Delta t = t_1 - t_0$, and $\underline{C}^F = (\underline{C}_1^F + \underline{C}_0^F)/2$. We solve eq 8 first, next eq 9, iterate these two equations until the concentrations of the radicals and fast species have converged, and then solve eq 10 for the slow species.

Differentiating eqs 8 and 9 with respect to λ gives equations for the sensitivities of the radicals and fast species:

$$\begin{pmatrix} \mathbf{J}_{RR} & \frac{1}{2}\mathbf{J}_{RF} \\ -\Delta t \cdot \mathbf{J}_{FR} & \mathbf{I} - \frac{\Delta t}{2}\mathbf{J}_{FF} \end{pmatrix} \begin{pmatrix} \underline{S}_1^R \\ \underline{S}_1^F \end{pmatrix} = \begin{pmatrix} -\frac{1}{2}\mathbf{J}_{RF} & -\mathbf{J}_{RS} \\ \mathbf{I} + \frac{\Delta t}{2}\mathbf{J}_{FF} & \Delta t \cdot \mathbf{J}_{FS} \end{pmatrix} \begin{pmatrix} \underline{S}_0^R \\ \underline{S}_0^S \end{pmatrix} \quad (11)$$

where \mathbf{I} is the identity matrix and the Jacobian matrix for the complete set of reaction rates is partitioned by species group as

$$\mathbf{J} = \begin{pmatrix} \mathbf{J}_{RR} & \mathbf{J}_{RF} & \mathbf{J}_{RS} \\ \mathbf{J}_{FR} & \mathbf{J}_{FF} & \mathbf{J}_{FS} \\ \mathbf{J}_{SR} & \mathbf{J}_{SF} & \mathbf{J}_{SS} \end{pmatrix}$$

Differentiating eq 10 yields the equation for the slow species

$$\underline{S}_1^S = \underline{S}_0^S + \Delta t \cdot (\mathbf{J}_{SR} \cdot \underline{S}_1^R + \mathbf{J}_{SF} \cdot \underline{S}_1^F + \mathbf{J}_{SS} \cdot \underline{S}_0^S) \quad (12)$$

with $\underline{S}^F = (\underline{S}_1^F + \underline{S}_0^F)/2$. We solve eqs 8–10 first, then eq 11, and last eq 12. The matrix on the left-hand side of eq 11 is the same for all parameters and need be evaluated and triangularized only once per time step. Also, no iteration is necessary in solving eqs 11 and 12.

Horizontal Advection Step. Horizontal advection is split into separate steps for the *x* and *y* directions. The governing equation for advection in the *x* direction is

$$\frac{\partial c}{\partial t} = -\frac{\partial}{\partial x}(uc) \quad (13)$$

where *u* is the wind speed. Because the equation for the sensitivities has the same form

$$\frac{\partial s}{\partial t} = -\frac{\partial}{\partial x}(us) \quad (14)$$

it would appear that the same numerical equations could be used to propagate the concentrations and sensitivities through the advection step. However, the Bott algorithm is defined by the equations

$$C_i^1 = C_i^0 - F_{i+1/2} + F_{i-1/2} \quad (15)$$

$$F_{i+1/2} = f_{i+1/2}^+(C_j^0) \cdot W_i - f_{i+1/2}^-(C_{j+1}^0) \cdot W_{i+1} \quad (16)$$

$$W_i = C_i^0 / \max[C_i^0, f_{i+1/2}^+(C_j^0) + f_{i-1/2}^-(C_j^0)] \quad (17)$$

Here C_i^1 and C_i^0 are the concentrations at t_1 and t_0 in grid cell *i*, and Δx is the length of cell *i*. The directional fluxes, e.g. $f_{i+1/2}^+(C_j^0)$, are polynomials of order *n* in the Courant number $\gamma_{i+1/2} = u_{i+1/2} \Delta t / \Delta x$ with coefficients that are linear combinations of C_j^0 , $j = i - (n-1)/2$ to $i + (n-1)/2$. Due to the flux limiting factors W_i , this algorithm is nonlinear in C_i^0 even though eq 13 is linear in *c*.

By carefully differentiating eqs 15–17, we obtain the equations for the sensitivities as

$$S_i^1 = S_i^0 - \Phi_{i+1/2} + \Phi_{i-1/2} \quad (18)$$

$$\Phi_{i+1/2} = \phi_{i+1/2}^+(S_j^0, C_j^0) - \phi_{i+1/2}^-(S_{j+1}^0, C_{j+1}^0) \quad (19)$$

If $C_i^0 \geq f_{i+1/2}^+(C_j^0) + f_{i-1/2}^-(C_j^0)$, then

$$\phi_{i+1/2}^+(S_j^0, C_j^0) = f_{i+1/2}^+(S_j^0) \quad (20)$$

If $C_i^0 < f_{i+1/2}^+(C_j^0) + f_{i-1/2}^-(C_j^0)$, then

$$\phi_{i+1/2}^+(S_j^0, C_j^0) = f_{i+1/2}^+(S_j^0) \cdot W_i + S_i^0 \cdot W_i^+ - [f_{i+1/2}^+(S_j^0) + f_{i-1/2}^-(S_j^0)] \cdot W_i \cdot W_i^+ \quad (21)$$

$$W_i^+ = f_{i+1/2}^+(C_j^0) / [f_{i+1/2}^+(C_j^0) + f_{i-1/2}^-(C_j^0)] \quad (22)$$

The differences between eqs 15–17 and eqs 18–22 address the nonlinearity introduced by the Bott algorithm. Consideration of nonlinearities introduced by the model algorithms is a subtle issue not presented in previous work (12, 19).

Lower Bounds. When the concentration of a species falls below a specified lower bound (10^{-6} ppb for most species), the model resets the concentration to the lower bound. This avoids possible inefficiency in solving for very low concentrations in the chemistry step. However, it also introduces small nonlinearities into the solution because the memory of preceding events is eliminated when the concentration is reset to its lower bound. Hence, $S_p(x_i, y_j, z_k, t)$ is reset to zero whenever $C_p(x_i, y_j, z_k, t)$ is reset to the lower bound for species *p*. Note that the sensitivity is reset only for a specific species, grid cell, and time. Overall, this approach should lead to no significant loss of information in a simulation because as the concentration becomes very small, the sensitivity also approaches zero.

Results and Discussion

One type of analysis we conducted is a comparison of sensitivities from the DDM with those from the BFM. This tests the consistency of the two techniques and gives an estimate of the accuracy of the sensitivities. To calculate the brute-force sensitivity S_p^{BFM} , we increased and decreased the parameter λ in separate model simulations, $C_p(\lambda = \delta)$ and $C_p(\lambda = -\delta)$, and used the equation

$$S_p^{\text{BFM}}|_{\lambda=0} = \frac{C_p(\lambda = \delta) - C_p(\lambda = -\delta)}{2\delta} = \left. \frac{\partial C_p}{\partial \lambda} \right|_{\lambda=0} + O(\delta^2) \quad (23)$$

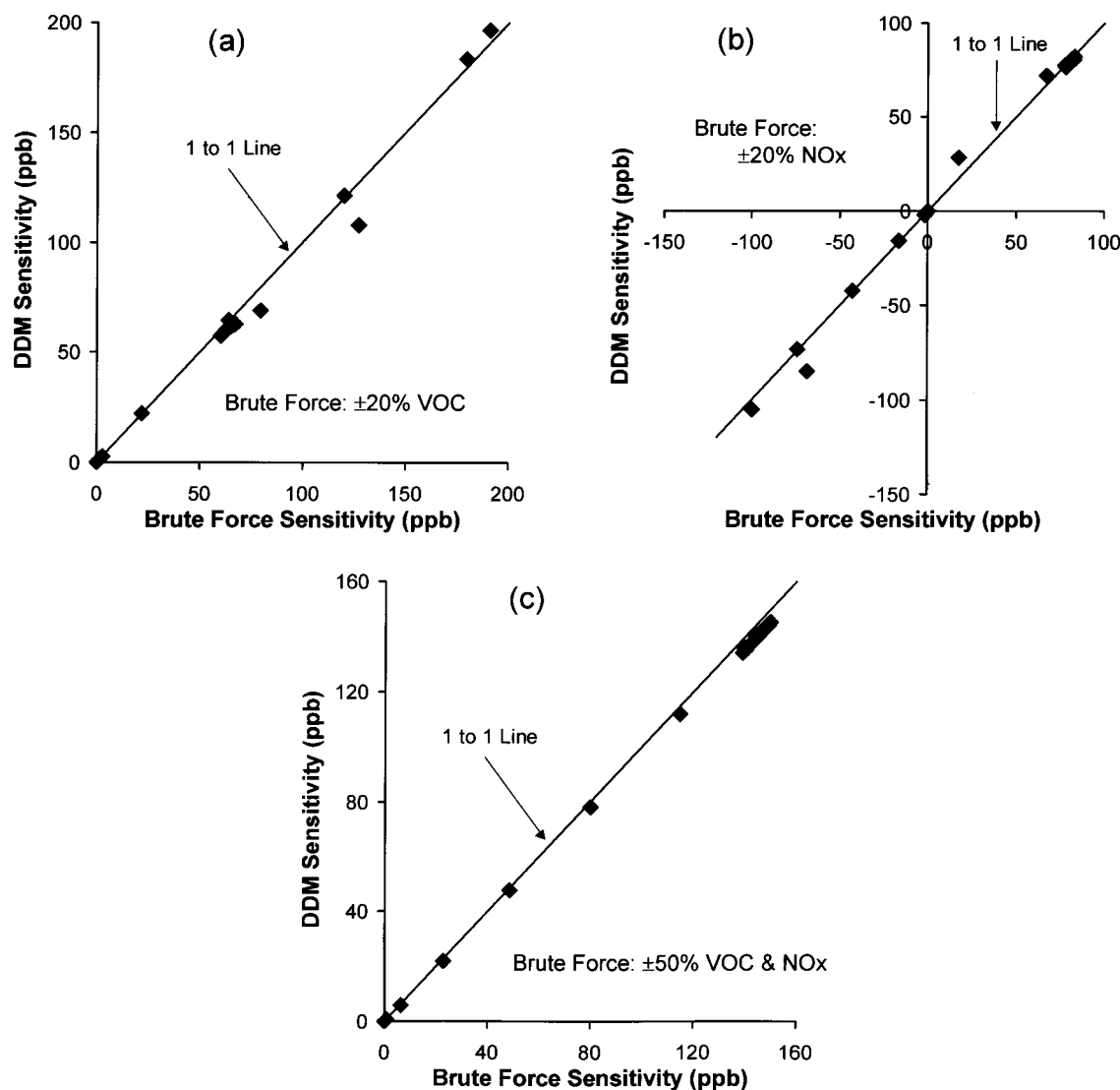


FIGURE 1. Comparison of DDM and brute-force sensitivities for the box model with the CB IV mechanism. Sensitivity of the ozone concentration (a) to varying the initial VOC concentration, (b) to varying the initial NO_x concentration, and (c) to varying the initial VOC and NO_x concentrations together. The points are the sensitivities at each hour over the 22-h simulation, and VOC/NO_x = 10 ppbC/ppb. Brute-force sensitivities were calculated with ±20% or ±50% changes in initial concentrations.

This is a two-sided approximation to the derivative such that the quadratic dependence of C_p on λ cancels and S_p^{BFM} is accurate through first-order in the perturbation δ . Our other type of analysis investigates the importance of the quadratic and higher-order dependence of C_p on λ or, equivalently, determines the range over which the first-order sensitivities provide useful information. For this analysis, we compare the concentration from a simulation in which λ is decreased, $C_p(\lambda = -\delta)$, with the linear approximation

$$C_p^{\text{lin}}(\lambda = -\delta) = C_p(\lambda = 0) - S_p^{\text{DDM}}|_{\lambda=0} \cdot \delta \quad (24)$$

Equation 24 is simply the first two terms of the Taylor series, eq 2, using the DDM sensitivity S_p^{DDM} . Below, we present selected results from these two types of analyses. For all results presented here, λ is a dimensionless scaling parameter (i.e., $g = I_0$ in eq 1, and $\lambda = 0.2$ corresponds to a 20% increase in the input).

Chemistry Simulations. To investigate the accuracy of the sensitivities for the chemistry step, we conducted simulations with the CB IV and SAPRC97 mechanisms in a box model. The model was run for 22 h, beginning at 6 A.M., with time-varying photolysis rates similar to those for Los

Angeles in June. For one set of simulations, the initial VOC and NO_x concentrations were 500 ppbC and 50 ppb, respectively (VOC/NO_x = 10 ppbC/ppb), and in the other set, the VOC and NO_x concentrations were 400 ppbC and 100 ppb (VOC/NO_x = 4 ppbC/ppb). The initial proportions of the VOC species were chosen to be similar to the proportions in morning, urban atmospheres and also to include contributions from all species. For the CB IV mechanism, the initial carbon fractions of the VOC species were as follows: PAR, 0.60; ETH, 0.05; OLE, 0.07; TOL, 0.049; XYL, 0.056; FORM, 0.025; ALD2, 0.05; MEOH, 0.01; ETOH, 0.02; ISOP, 0.025; NR, 0.045. (PAR, ETH, OLE, TOL, XYL, FORM, and ALD2 represent various types of carbon atoms, and MEOH, ETOH, ISOP, and NR are methanol, ethanol, isoprene, and nonreactive carbon atoms, respectively (25).) The model did not include emissions of any species, dilution, or deposition.

Figure 1 presents a comparison of the DDM and BFM sensitivities for the simulation with the CB IV mechanism and initial VOC/NO_x = 10. Using ±20% changes ($\delta = 0.2$) in eq 23 to calculate the brute-force sensitivities, there is good agreement between the DDM and BFM for the sensitivity of ozone with respect to initial VOC and with respect to initial

TABLE 1. CPU Time for Chemistry, Advection, and Diffusion Simulations

no. of sensitivity parameters	CB IV ^c		SAPRC97 ^c	
	total time (s) ^a	time per parameter ^b	total time (s) ^a	time per parameter ^b
0 ^d	0.052		0.165	
1	0.097	0.87	0.297	0.80
2	0.102	0.48	0.307	0.43
10	0.154	0.20	0.477	0.19
20	0.223	0.16	0.693	0.16

no. of sensitivity parameters	2D advection ^e		3D advection and diffusion ^e	
	total time (s) ^a	time per parameter ^b	total time (s) ^a	time per parameter ^b
0 ^d	6.0		74	
1	11.3	0.90	124	0.68
2	15.7	0.82	160	0.59
20	67.5	0.52	754	0.46

^a Includes time for both concentrations and sensitivities. ^b Normalized to time required for concentrations only. ^c Simulation of 22 h for the box model. ^d Concentrations only. ^e Simulation of one rotation of the hill about the center of the grid.

NO_x (Figure 1, parts (a) and (b), respectively). Additional simulations show that the agreement improves, as the changes used in the BFM become smaller. For example, the average absolute value of the difference between the DDM and BFM sensitivities for ∂O₃/∂(initial VOC) is 35.5, 3.8, and 0.3 ppb when changes of ±50%, ±20%, and ±5%, respectively, are used in eq 23. (The comparison for ±20% is shown in Figure 1(a); comparisons of ∂O₃/∂(initial VOC) using ±50% and ±5% changes in eq 23 are not shown.) Figure 1(c) gives the comparison between the DDM and BFM for the sensitivity of ozone with respect to a simultaneous change in initial VOC and NO_x. (Here, both initial concentrations are varied by the same fractional amount, whereas in Figure 1(a),(b) only one initial concentration is varied.) The agreement in Figure 1(c) is better than in Figure 1(a),(b), even though changes of ±50% were used for the BFM in Figure 1(c). This indicates that the response of ozone to simultaneous changes in VOC and NO_x is more nearly linear than the response to changes in either VOC or NO_x separately, in these simulations. Results for the simulations with initial VOC/NO_x = 4 are similar to those in Figure 1.

The CPU time to compute the concentrations and sensitivities for 1, 2, 10, and 20 parameters is given in Table 1. Also shown in the table is the time per sensitivity parameter, which is (T_n - T₀)/nT₀, where T_n is the total time to calculate the concentrations and sensitivities for n parameters together and T₀ is the time for the concentrations only. For both the CB IV and SAPRC97 mechanisms, the time per sensitivity parameter is 16% of the time required for the concentrations, if sensitivities are calculated for 20 or more parameters together. Equivalently, calculating the sensitivity to one parameter is up to 6 times faster than calculating the concentrations. This efficiency improvement arises because eqs 8–10 involve iteration but eqs 11 and 12 do not and because the matrix on the left-hand side of eq 11 needs to be triangularized only once, regardless of the number of parameters being considered.

Advection Simulations. We tested the sensitivities for the horizontal advection step by simulating a hill of concentration rotating around the center of a 100 × 100 grid of cells using the Bott algorithm. One rotation of the hill requires 314 time steps in this simulation, and the maximum Courant number in the two-dimensional (2D) grid is 0.97. The initial concentration distribution is

$$c(x,y;\lambda_1,\lambda_2) = 3(1 + \lambda_1) \left[\cos\left(\frac{2\pi}{10(1 + \lambda_2)}r\right) + 1 \right] + 4, \quad r \leq 5$$

$$= 4, \quad r > 5$$

$$r = [(x - 75)^2 + (y - 50)^2]^{1/2} \quad (25)$$

For the base-case values of the parameters (λ₁ = λ₂ = 0), this is a cosine hill with a diameter of 10 cells and a height of 6 atop a background concentration of 4. (The concentration units are arbitrary.) We calculated the sensitivity with respect to λ₁, which adjusts the height of the hill, and with respect to λ₂, which adjusts the diameter of the hill. This is a relatively stringent test since the diameter of the hill is only 10 cells. After one rotation, the maximum concentration (hill plus background) is 9.36.

Figure 2 gives the comparison of the DDM and BFM sensitivities in the region of the hill, and there is excellent agreement for ∂C/∂λ₁ (Figure 2(a)). Because the initial concentration depends linearly on λ₁, the only nonlinear dependence of the simulated concentration C on λ₁ is the nonlinearity introduced by the Bott algorithm. By contrast, the initial concentration and therefore also the simulated concentration have a strong nonlinear dependence on λ₂, in addition to any nonlinearity from the Bott algorithm. Hence, the agreement between the DDM and BFM is not as close for ∂C/∂λ₂ as ∂C/∂λ₁, but the BFM approaches the DDM as the changes used in eq 23 become small (Figure 2(b),(c)).

We also simulated 3D advection and diffusion together. In this simulation, there is a 100 × 100 × 5 grid, and the hill begins in the second layer with the concentration distribution of eq 25. The hill then makes one rotation in the horizontal plane while moving upward two layers and undergoing diffusion. The agreement between the DDM and BFM for sensitivities with respect to λ₁ and λ₂ is very similar to that in Figure 2.

Table 1 gives the CPU times to obtain increasing numbers of sensitivities in the 2D and 3D simulations. In both tests, the time per sensitivity parameter is about half the time required to calculate the concentrations if sensitivities are calculated for 20 or more parameters. This increase in efficiency occurs because some quantities are the same for all sensitivities and thus need be calculated only once, e.g. W_i and W_i⁺ in eq 21. Also, matrices in the implicit algorithms for vertical advection and diffusion need be triangularized only once for all sensitivities.

CAMx Simulations. We applied the complete model with the DDM to simulate the ozone episode of July 7–13, 1995 in the Lake Michigan region. Figure 3 presents the modeling domain, which consists of a coarse grid of cells, approximately 12 km × 12 km, and a nested fine grid of cells, approximately 4 km × 4 km. (The domain and cells are actually defined in latitude/longitude coordinates.) There are 58 × 93 cells in the horizontal coarse grid, 81 × 120 cells in the fine grid, and 7 vertical layers in both grids. We ran the simulation with the coarse grid only on July 7–9, since these are initialization days. On the days with the highest ozone concentrations, July 10–13, we used both the coarse and fine grids.

We took the inputs required by CAMx from previous work in modeling this episode (31). Briefly, a prognostic meteorological model (Regional Atmospheric Modeling System 3a (32)) with four-dimensional data assimilation was employed to develop the wind field and other meteorological inputs. Biogenic emissions were estimated using the Biogenic Emissions Inventory System 2 (33). Anthropogenic emissions were estimated with MOBILE5a (34) and other models and data available through December 1998. To obtain the initial and boundary concentrations, ozone formation was simulated for an extended time period over the entire eastern U.S. with a 36 km × 36 km grid. Concentrations were then

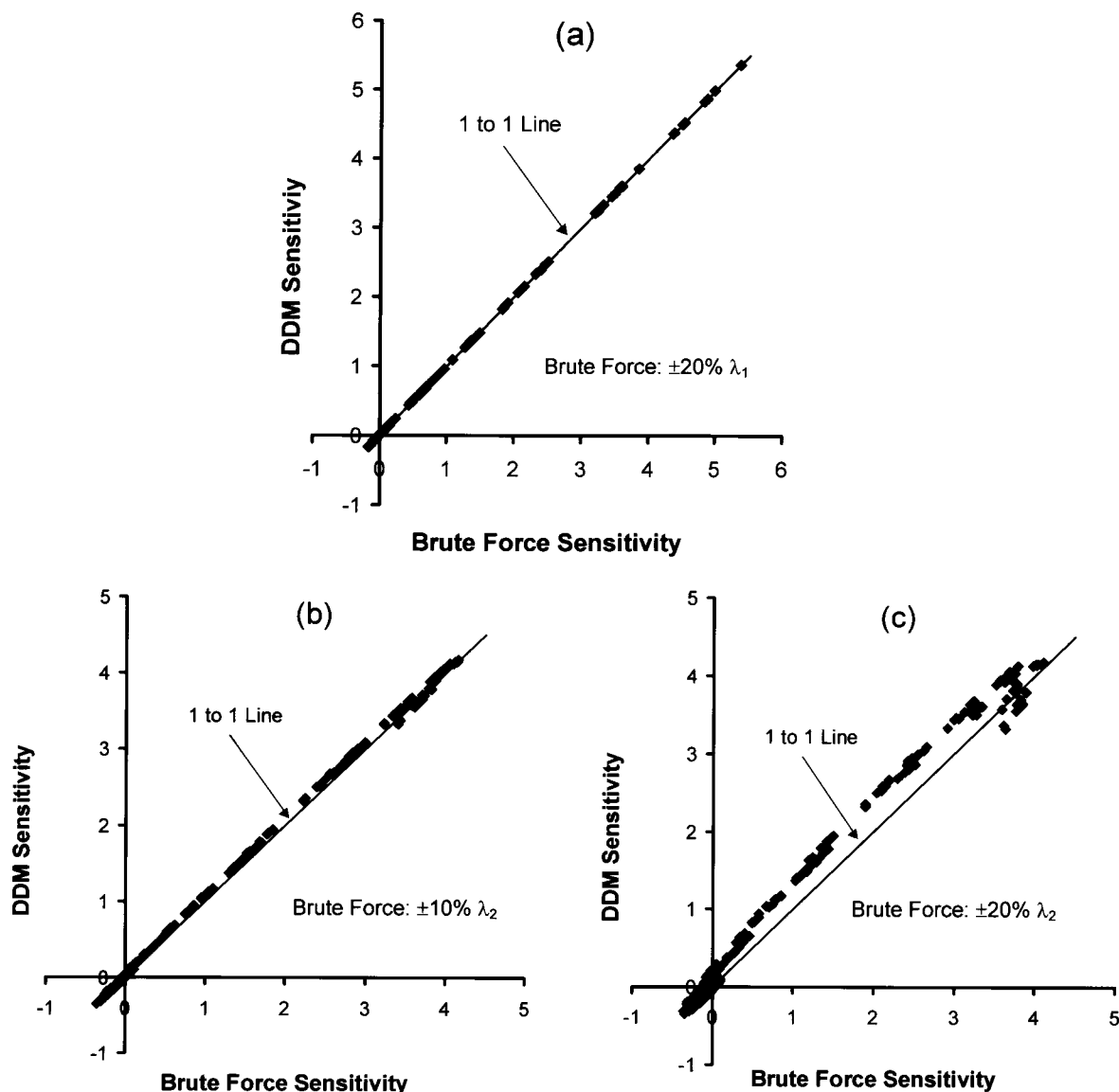


FIGURE 2. Comparison of DDM and brute-force sensitivities after one rotation of the hill in the simulation of 2D advection. Sensitivity of the concentration (a) to the height of the hill and (b, c) to the diameter of the hill. Points are shown for a 31×31 grid of cells centered on the peak concentration.

extracted from this larger-scale simulation to use as initial and boundary concentrations for the domain in Figure 3. The meteorological and emissions inputs were originally developed for a 4-km grid covering the entire domain in Figure 3. We aggregated these inputs as necessary to create inputs for the 12-km grid. For all simulations, we used the CB IV mechanism.

Table 2 summarizes the emissions in the modeling domain on July 10–13. Biogenic VOC emissions are clearly large, representing 75–82% of total VOC emissions. Though biogenic NO_x emissions are not large, neither are they negligible at 12–16% of total NO_x emissions. The distribution of ozone predicted with these emissions is quite complex, as shown in Figure 4 for July 13, 1500–1600 CST. (These and all other results discussed below are for the surface layer of the model.) There is a large ozone plume downwind of the Chicago region, smaller plumes downwind of St. Louis, Louisville, and Cincinnati, plus other areas of ozone above 120 ppb.

Figure 5 provides examples of results obtained with the DDM and BFM, namely the sensitivity of ozone on July 13, 1500–1600 to all area-source VOC emissions and the

sensitivity to all area-source NO_x emissions. (These are the sensitivities with respect to changing both biogenic and anthropogenic area-source emissions on all days.) The spatial distribution of the sensitivity to area-source VOC emissions, Figure 5(a), (b), is similar to the spatial distribution of ozone, Figure 4. However, the spatial distribution of the sensitivity to area-source NO_x , Figure 5(c), (d), is less closely related to ozone. There are some regions of negative sensitivity to VOC emissions in the southern part of the domain, which appear to be due to high biogenic isoprene emissions. The sensitivity to area-source NO_x emissions is negative in some urban locations (Chicago, Detroit, Louisville, Cincinnati, Columbus, Indianapolis) and positive elsewhere.

Accuracy of Sensitivities. To examine the accuracy of the DDM in the complete model, we calculated sensitivities by the BFM using $\pm 20\%$ changes in eq 23. As shown in Figure 5, the agreement between the DDM and BFM for the spatial distribution of the sensitivities is excellent. Figure 6 provides a sensitive comparison of the magnitude of the BFM and DDM sensitivities for all surface-layer grid cells in the modeling domain. The agreement is very good for both the sensitivity to area-source VOC emissions and to area-source

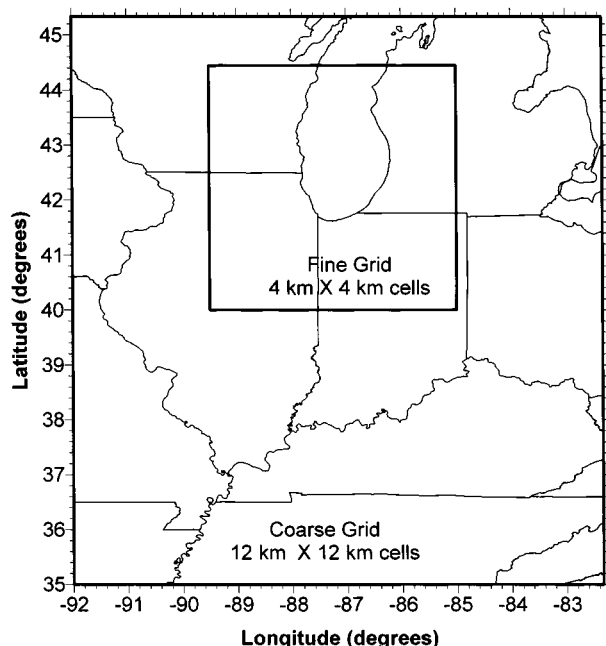


FIGURE 3. Midwest modeling domain with outer coarse grid and nested fine grid.

TABLE 2. Emissions over the Modeling Domain on July 10–13, 1995^a

source type	date	VOC (mol/day) ^{b,c}	NO _x (mol/day) ^c	CO (mol/day) ^c
point sources	July 10–13	3.68 E7	1.49 E8	1.15 E8
anthropogenic	July 10	5.96 E8	1.60 E8	1.51 E9
area sources	July 11	6.08 E8	1.61 E8	1.53 E9
	July 12	6.17 E8	1.62 E8	1.54 E9
	July 13	6.35 E8	1.63 E8	1.58 E9
biogenic sources	July 10	1.90 E9	4.37 E7	0
	July 11	2.42 E9	4.92 E7	0
	July 12	2.75 E9	5.35 E7	0
	July 13	3.10 E9	5.87 E7	0

^a Includes both coarse and fine grids. All days are weekdays. ^b Moles of carbon atoms. ^c E denotes exponent of 10.

NO_x emissions, with the regression lines being nearly one-to-one lines. Due to numerical roundoff errors, the BFM loses accuracy if the concentrations in the numerator of eq 23 differ only in the last few digits of the single-precision arithmetic used in these simulations. However, the agreement is good even for small sensitivities where the BFM accuracy decreases, as shown in Figure 6(b). We also compared the DDM and BFM for the sensitivity to point-source NO_x emissions, and the level of agreement is the same as that in Figures 5 and 6. (These results are in the Supporting Information for this paper.)

In most sensitivity analyses, the sensitivities of the higher ozone concentrations are of particular importance, since these are the concentrations that must be reduced to achieve the air quality standard. Table 3 presents the difference between the BFM and DDM sensitivities for those grid cells and hours with ozone concentrations above 80 ppb. The average absolute (value of the) difference is ≤ 0.23 ppb, ≤ 0.014 ppb and ≤ 0.002 ppb for sensitivities with respect to area-source emissions, lateral boundary concentrations, and initial concentrations, respectively. In all cases, the average absolute difference is $\leq 1\%$ of the average absolute DDM sensitivity. The results in Table 3 were obtained using $\delta = 0.2$ in eq 23 to calculate the BFM sensitivities, but we also calculated the sensitivity to area-source VOC emissions using

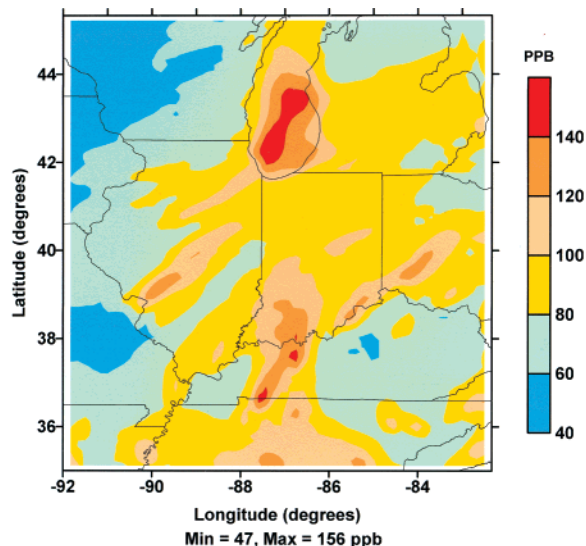


FIGURE 4. Predicted hourly average ozone concentration for July 13, 1995, 1500–1600 CST.

$\delta = 0.3, 0.1,$ and 0.02 . These results show that the BFM sensitivities steadily converge toward the DDM sensitivities down to $\delta = 0.1$. At $\delta = 0.1$, the average absolute difference between the DDM and BFM is about half that in Table 3. For $\delta < 0.1$, however, numerical roundoff errors become important for the BFM, and the agreement between the DDM and BFM for $\delta = 0.02$ is no better than for $\delta = 0.1$. Overall, this convergence test, Figures 5 and 6 and Table 3 indicate that the DDM results accurately represent the first-order sensitivity of the numerical model (eq 4), to the extent allowed by the precision of the computations.

Accuracy of Ozone Changes. The value of first-order sensitivities is in predicting the impact of changes in model inputs on ozone and other species via eq 24. The accuracy of this linear approximation as a function of the magnitude of the input changes determines the range over which the sensitivities provide useful information. Figure 7 presents a comparison of ozone changes predicted from eq 24 and ozone changes obtained by actually reducing area-source emissions by 40%. As determined by the regression lines, the predicted and actual ozone changes have high correlation, but the predicted changes are on average 7–16% smaller in magnitude than the actual changes. For nearly all grid cells, the predicted ozone change has the same sign as the actual ozone change (directionally correct). The only exceptions are in Figure 7(b) for a few grid cells with small ozone changes. The agreement is best for reductions in VOC and NO_x emissions together (Figure 7(c)), consistent with the results of the box-model test of chemistry in Figure 1. Also, the ozone concentration in the box model test generally has negative second-order sensitivities with respect to initial VOC and NO_x. This suggests that the second-order terms omitted in eq 24 are likely negative, which would explain why the predicted ozone change in Figure 7 is smaller in magnitude than the actual change.

Table 4 contains additional comparisons between predicted and actual ozone changes resulting from reductions in emissions and initial and lateral boundary concentrations. We determined the errors in the predicted changes for those grid cells and hours having ozone concentrations > 80 ppb in the base-case simulation. For 40% reductions in area-source VOC or NO_x emissions, the average absolute error is 15–20% of the average absolute ozone change. For a 40% reduction in both area-source VOC and NO_x emissions, 40% reductions in lateral boundary concentrations, or 100% reductions in initial concentrations, the average error is $\leq 10\%$

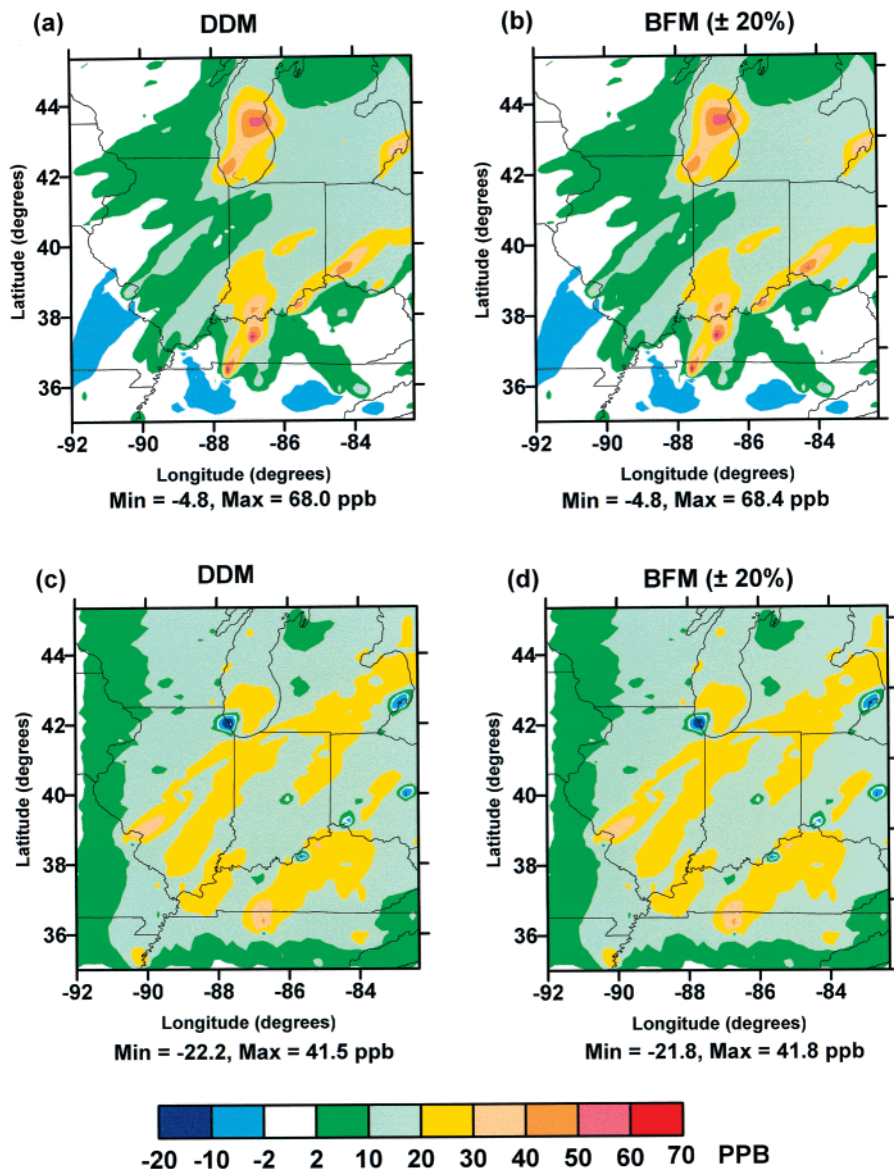


FIGURE 5. Sensitivity of ozone to all area-source emissions, both biogenic and anthropogenic, as obtained by the DDM and BFM for July 13, 1995, 1500–1600 CST: (a) and (b) VOC emissions and (c) and (d) NO_x emissions.

TABLE 3. Difference between DDM and Brute-Force Sensitivities, Averaged over Grid Cells and Hours with Ozone Greater than 80 ppb^a

sensitivity	average absolute value of difference (ppb) ^b			
	July 10	July 11	July 12	July 13
area-source VOC	0.23 (20.)	0.19 (19.)	0.17 (17.)	0.11 (14.)
area-source NO_x	0.16 (13.)	0.10 (12.)	0.10(14.)	0.09 (14.)
lateral-boundary VOC	0.0056 (4.0)	0.0064 (3.6)	0.0081 (3.3)	0.014 (3.1)
lateral-boundary NO_x	0.0028 (0.42)	0.0034 (0.58)	0.0037 (0.75)	0.0056 (1.6)
initial VOC	0.0021 (1.9) ^c			
initial NO_x	0.0006 (0.2) ^c			

^a Brute-force sensitivities were calculated with $\pm 20\%$ perturbations in eq 23. ^b The average absolute value of the DDM sensitivity is given in parentheses. ^c Results are for July 7, averaged over cells and hours with ozone > 60 ppb because the sensitivity to initial concentrations is low after the first day and the ozone is lower on July 7 than other days.

of the average ozone change. The accuracy needed for the predicted ozone changes depends on the particular questions to be answered. Nevertheless, the results in Figure 7 and Table 4 indicate that the first-order sensitivities provide useful information on ozone changes for reductions up to 40% in emissions and initial and boundary concentrations. To some extent, this conclusion is specific to the model, episode, and geographic domain we have studied. However, there is a

wide range of concentrations and emissions across the domain and areas of VOC-limited and NO_x -limited chemistry, so this episode should be a good test of the accuracy of the predicted ozone changes for models using the CB IV mechanism.

We examined the simulations in detail and found three major sources of nonlinearity in the ozone response. First, ozone is titrated by NO at night. If a parameter λ increases

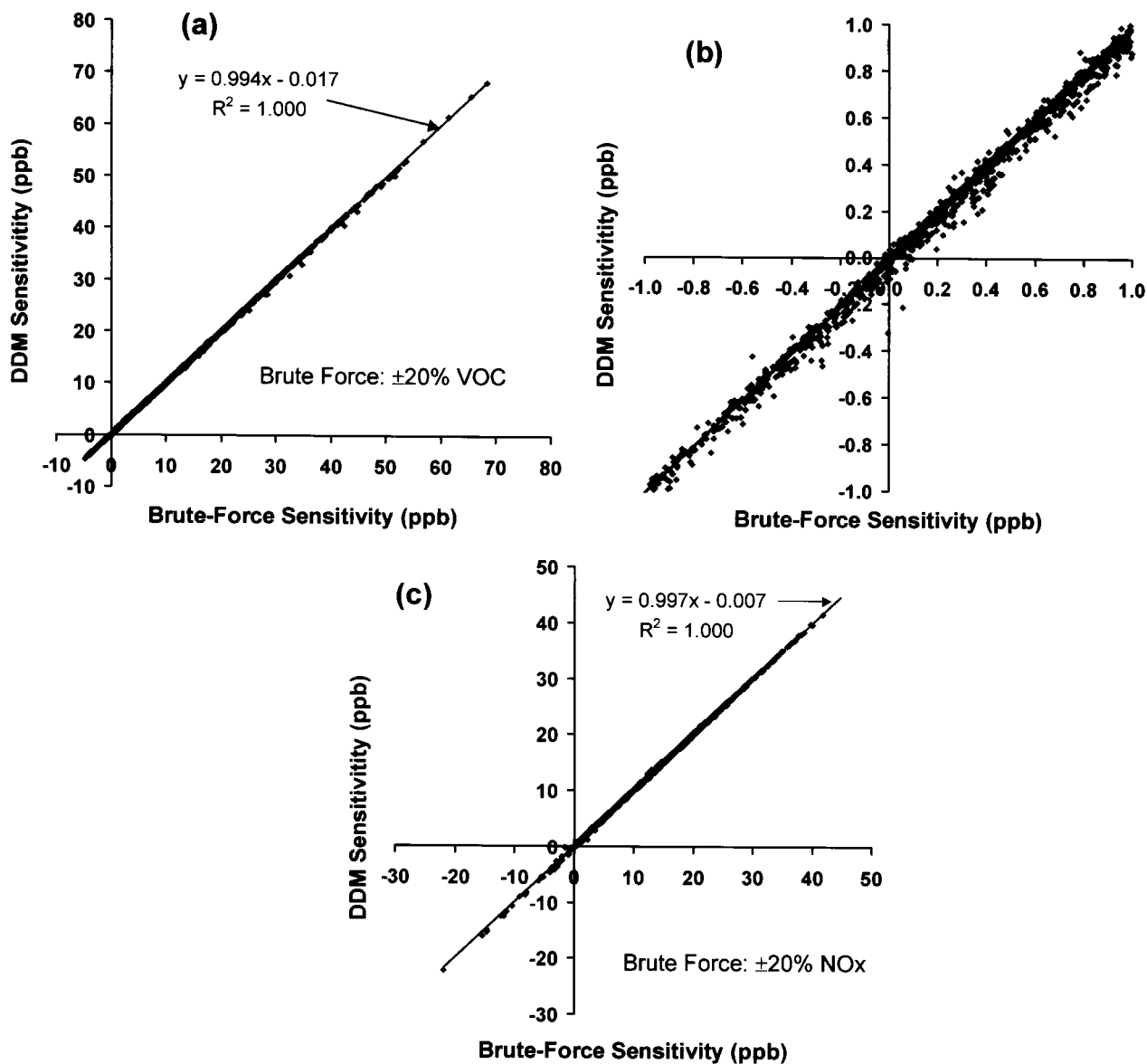


FIGURE 6. Comparison of DDM and brute-force sensitivities for all grid cells in the modeling domain, July 13, 1995, 1500–1600 CST. Sensitivity of ozone (a), (b) to all area-source VOC emissions and (c) to all area-source NO_x emissions. Part (b) is an expansion about the origin of (a).

the NO concentration in a particular grid cell, the ozone concentration decreases until it becomes zero at some value λ_0 and remains zero for $\lambda > \lambda_0$. The ozone response is approximately linear for $\lambda < \lambda_0$ and exactly linear for $\lambda > \lambda_0$. However, because $\partial O_3 / \partial \lambda$ is discontinuous at λ_0 , the ozone response is nonlinear whenever a change in λ crosses λ_0 . Second, the ozone response in a grid cell is approximately linear when the chemistry remains either VOC-limited or NO_x-limited over the variation in λ . However, if the variation in λ causes the chemistry to switch from being VOC-limited to NO_x-limited or vice versa, the ozone response generally becomes much more nonlinear. Since the ozone plume downwind of a large emission region usually changes from VOC-limited to NO_x-limited at some afternoon hour, the ozone concentrations near the location and hours of this transition respond nonlinearly to changes in the upwind emissions. Finally, the concentrations at the edges of sharply defined ozone plumes (e.g., downwind of Chicago) have a more nonlinear response to parameter changes. This is most likely due to application of the flux limiting factors in the Bott algorithm.

Efficiency. We have run simulations of the ozone episode on several computers, and Table 5 gives the CPU times for different numbers of sensitivities on the fastest and slowest machines. When sensitivities are calculated for 20 parameters simultaneously, the time per sensitivity parameter is 40–55% of the time required to calculate the concentrations alone or, equivalently, the speed is 1.8–2.5 times faster. The information in Table 1 along with the fraction of time devoted to chemistry and to advection and diffusion in simulations of the concentrations can be used to estimate an expected time per sensitivity parameter for the ozone episode. The expected time per parameter is 0.34 for the personal computer and 0.30 for the workstation for 20 parameters. The most likely explanation for the slower than expected times in Table 5 is that the time needed to gather information from the array of sensitivity coefficients becomes significant as the number of grid cells in the modeling domain becomes large. There are opposing requirements in storing sensitivities for a grid model because the optimum approach for advection/diffusion would group together the sensitivities of a given species for all grid cells, whereas for chemistry it is best to

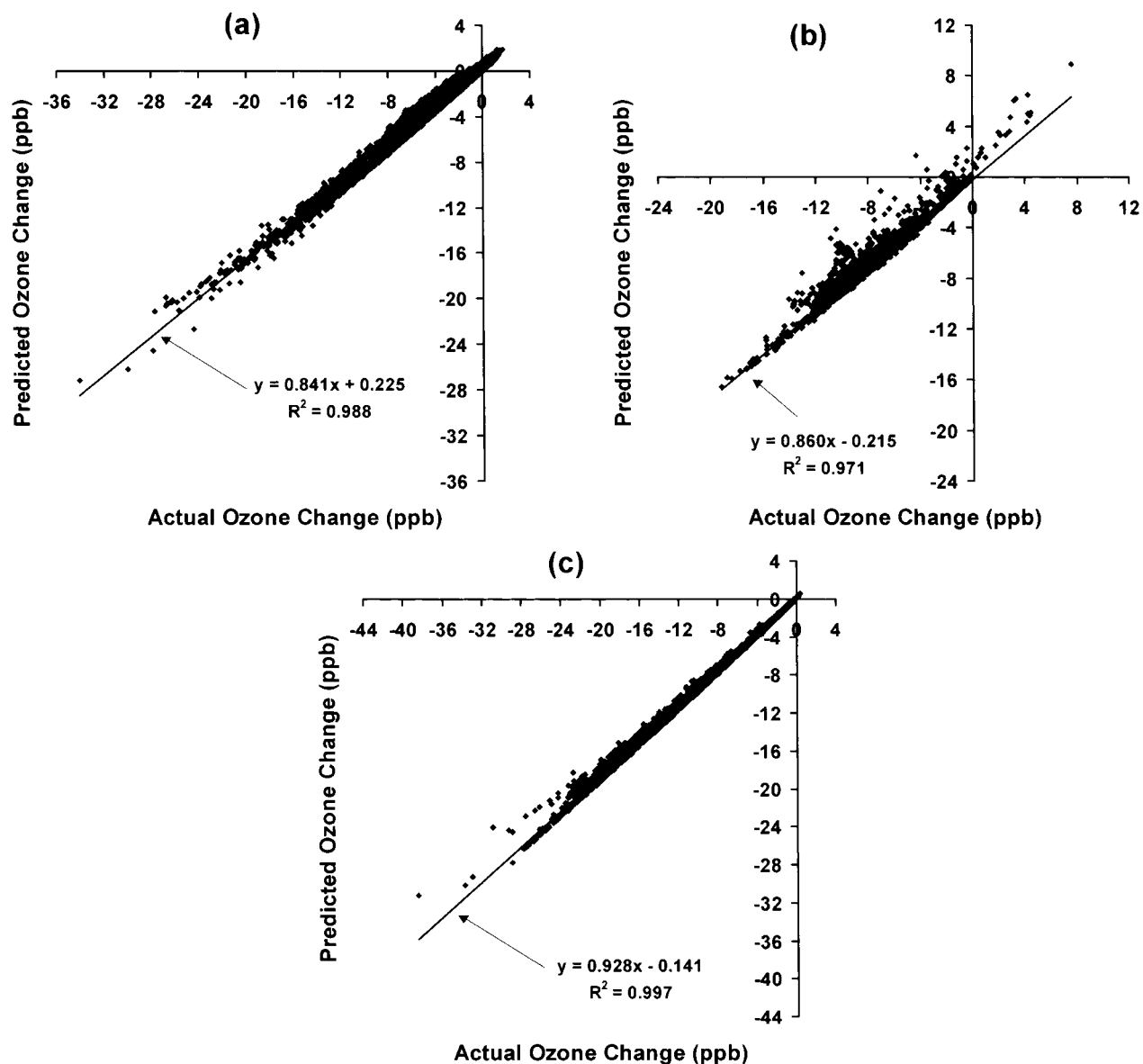


FIGURE 7. Comparison of predicted ozone changes from a linear expression using the DDM sensitivity and actual changes from model simulations with reduced emissions. Points are for all grid cells in the modeling domain, July 13, 1995, 1500–1600 CST: (a) 40% reduction in all area-source VOC emissions; (b) 40% reduction in all area-source NO_x emissions; and (c) 40% reduction in both area-source VOC and NO_x emissions.

group together the sensitivities of all species in a given cell. Consequently, there will always be a step when sensitivity coefficients must be gathered inefficiently from throughout a very large array. The time per sensitivity parameter may then be greater than expected by an amount dependent on the machine architecture (e.g., cache size, speed of memory access).

Other Sensitivity Methods. While ADIFOR has not been applied to a 3D model, it has been applied to chemistry box models (16, 35, 36) and advection models (17). Table 6 compares the CPU time per sensitivity parameter for these applications of ADIFOR to our results for similar applications of DDM (Table 1). The DDM is more efficient for both the advection and chemistry examples by a factor of 5 or more. There are two approaches to applying ADIFOR, the black-box approach and the variational approach, with the latter being more efficient (35). However, the DDM appears more efficient even for the one application of ADIFOR that clearly employed the variational approach. (It is unclear which approach was used for ADIFOR in the other two studies.) Applying the DDM to specific algorithms and computer code

as we have done requires more human effort than applying ADIFOR. Nevertheless, this effort appears justified for 3D models because of the substantial increase in efficiency. Tests in ref 17 suggest that ADIFOR gives accurate results. However, a comparison of the DDM and ADIFOR on identical test cases would be necessary to determine if there is any difference in accuracy between these two methods.

In the first application of the DDM-3D (19), the time per sensitivity parameter was 0.04 when sensitivities were calculated for 20 parameters together. This is much less than the time per parameter for the DDM in our application (Table 5). However, in another application of the DDM-3D (2), the time per sensitivity parameter was 0.40 when sensitivities were calculated for five parameters, and this is close to the time per parameter for the DDM, 0.52–0.70. The difference in time per parameter between the DDM and DDM-3D may be due to several factors. The greatest gain in efficiency for the DDM is in the chemistry step. In calculating the concentrations alone, CAMx requires a relatively small fraction of time for the chemistry step, about 60% of the total time. Consequently, there will be less overall efficiency gain

TABLE 4. Error in Ozone Changes Predicted Using DDM Sensitivities, Averaged over Grid Cells and Hours with Ozone Greater than 80 ppb^a

input	% reduction	average absolute value of error (ppb) ^b			
		July 10	July 11	July 12	July 13
area-source VOC	20	0.44 (4.38)	0.42 (4.30)	0.40 (3.68)	0.32 (3.08)
	30	1.03 (6.93)	0.98 (6.79)	0.93 (5.85)	0.74 (4.88)
	40	1.90 (9.76)	1.81 (9.57)	1.71 (8.27)	1.37 (6.87)
area-source NO _x	20	0.27 (2.68)	0.24 (2.68)	0.24 (3.02)	0.21 (3.07)
	30	0.65 (4.13)	0.57 (4.18)	0.55 (4.69)	0.49 (4.76)
	40	1.21 (5.67)	1.06 (5.82)	1.02 (6.50)	0.90 (6.57)
area-source VOC and NO _x	20	0.25 (6.18)	0.25 (6.41)	0.24 (6.21)	0.19 (5.67)
	30	0.58 (9.48)	0.59 (9.82)	0.56 (9.51)	0.44 (8.66)
	40	1.09 (13.00)	1.09 (13.40)	1.04 (12.96)	0.81 (11.78)
lateral boundary VOC	20	0.01 (0.80)	0.01 (0.72)	0.02 (0.67)	0.03 (0.65)
	40	0.05 (1.65)	0.04 (1.46)	0.06 (1.37)	0.14 (1.37)
lateral boundary NO _x	20	0.002 (0.09)	0.003 (0.12)	0.003 (0.15)	0.008 (0.33)
	40	0.01 (0.17)	0.01 (0.24)	0.01 (0.31)	0.03 (0.68)
initial VOC	100	0.12 (2.04) ^c			
initial NO _x	100	0.02 (0.22) ^c			

^a Prediction from eq 24 compared to actual ozone change from simulation with reduced input. ^b The average absolute value of the actual ozone change is given in parentheses. ^c Results are for July 7, averaged over cells and hours with ozone > 60 ppb.

TABLE 5. CPU Time for Full 3D Model in a Simulation of July 7 Using 12 km Grid

no. of sensitivity parameters	personal computer ^a		workstation ^b	
	total time (min) ^c	time per parameter ^d	total time (min) ^c	time per parameter ^d
0 ^e	26.3		51.8	
1	68.3	1.59	108.0	1.09
2	81.4	1.04	130.8	0.76
5	118.8	0.70	185.4	0.52
10	184.4	0.60	276.6	0.43
20	316.3	0.55	466.5	0.40

^a Compaq Pentium III, 550 MHz processor, Linux operating system. ^b Sun Ultra 30, 333 MHz processor. ^c Includes time for both concentrations and sensitivities. ^d Normalized to time required for concentrations only. ^e Concentrations only.

TABLE 6. Comparison of CPU Time Per Parameter for DDM and ADIFOR

ADIFOR		DDM	
no. of sensitivity parameters	time per parameter ^a	no. of sensitivity parameters	time per parameter ^a
2D Advection with Bott Algorithm			
1	5.1 ^b	1	0.90
Chemistry Box Model			
84	0.96 ^c	20	0.16
375	1.2 ^d		

^a Normalized to time required for concentrations only. ^b Reference 17. ^c Reference 35, Variational Approach. ^d Reference 36.

in applying the DDM to CAMx than to other models that use a higher fraction of time for the chemistry step. Second, the DDM-3D uses a different algorithm and time step to propagate the sensitivities through the chemistry step than the algorithm and time step for the concentrations, which may result in greater speed but less accurate sensitivities than the DDM. Finally, the number of grid cells varies across the applications, which may influence the efficiency via the time required to access the sensitivities. The number of cells in our application, ~106 000, is larger than in the applications of the DDM-3D, 12 000 (19) and ~65 000 (2).

There has been no detailed presentation of the accuracy or efficiency of the adjoint method applied to air quality models. However, a recent implementation of this method

in a 3D model (18) required an advanced parallel computer running 42 to 120 processors, which suggests large CPU times.

Acknowledgments

The authors gratefully acknowledge the support of the Coordinating Research Council under Project A-29 and the additional support provided by ENVIRON International Corp. and the General Motors R&D Center.

Supporting Information Available

Figures SI-1 and SI-2 compare the BFM and DDM sensitivities to point-source NO_x emissions. This material is available free of charge via the Internet at <http://pubs.acs.org>.

Literature Cited

- Dunker, A. M. *Atmos. Environ.* **1980**, *14*, 671–679.
- Mendoza-Dominguez, A.; Wilkinson, J. G.; Yang, Y.-J.; Russell, A. G. *J. Air Waste Manage. Assoc.* **2000**, *50*, 21–31.
- Gao, D.; Stockwell, W. R.; Milford, J. B. *J. Geophys. Res.* **1995**, *100*, 23153–23166.
- Carter, W. P. L.; Atkinson, R. *Environ. Sci. Technol.* **1989**, *23*, 864–880.
- Yang, Y.-J.; Stockwell, W. R.; Milford, J. B. *Environ. Sci. Technol.* **1995**, *29*, 1336–1345.
- Glasson, W. A.; Dunker, A. M. *Environ. Sci. Technol.* **1989**, *23*, 970–978.
- Mendoza-Dominguez, A.; Russell, A. G. *Environ. Sci. Technol.* **2000**, *34*, 4974–4981.
- Dunker, A. M. *Atmos. Environ.* **1986**, *20*, 479–486.
- Vuilleumier, L.; Harley, R. A.; Brown, N. J. *Environ. Sci. Technol.* **1997**, *31*, 1206–1217.
- Gao, D.; Stockwell, W. R.; Milford, J. B. *J. Geophys. Res.* **1996**, *101*, 9107–9119.
- Chen, L.; Rabitz, H.; Considine, D. B.; Jackman, C. H.; Shorter, J. A. *J. Geophys. Res.* **1997**, *102*, 16201–16214.
- Dunker, A. M. *Atmos. Environ.* **1981**, *15*, 1155–1161.
- Dunker, A. M. *J. Chem. Phys.* **1984**, *81*, 2385–2393.
- Kramer, M. A.; Calo, J. M.; Rabitz, H. *Appl. Math. Modelling* **1981**, *5*, 432–441.
- Bischof, C.; Carle, A.; Corliss, G.; Griewank, A.; Hovland, P. *Sci. Programming* **1992**, *1*, 11–29.
- Carmichael, G. R.; Sandu, A.; Potra, F. A. *Atmos. Environ.* **1997**, *31*, 475–489.
- Hwang, D.; Byun, D. W.; Odman, M. T. *Atmos. Environ.* **1997**, *31*, 879–888.
- Elbern, H.; Schmidt, H. *J. Geophys. Res.* **1999**, *104*, 18583–18598.
- Yang, Y.-J.; Wilkinson, J. G.; Russell, A. G. *Environ. Sci. Technol.* **1997**, *31*, 2859–2868.
- Yarwood, G.; Morris, R.; Emery, C.; Wilson, G.; *Proceedings of the 91st Annual Meeting of the Air & Waste Management Association*; Air & Waste Management Association: Pittsburgh, PA, 1998; Paper 98-MP2B.06.

- (21) *User's Guide – Comprehensive Air Quality Model with Extensions (CAMx), version 3.00*; Environ International Corp.: Novato, CA, December, 2000.
- (22) CAMx v. 3.00 is available at <http://www.camx.com>.
- (23) Dunker, A. M.; Yarwood, G.; Ortmann, J. P.; Wilson, G. M. *Environ. Sci. Technol.*, in press.
- (24) Bott, A. *Mon. Wea. Rev.* **1989**, *117*, 1006–1015.
- (25) Gery, M. W.; Whitten, G. Z.; Killus, J. P.; Dodge, M. C. *J. Geophys. Res.* **1989**, *94*, 12925–12956.
- (26) Carter, W. P. L. *Atmos. Environ.* **1996**, *30*, 4275–4290.
- (27) Carter, W. P. L.; Lu, D.; Malkina, I. L. *Environmental Chamber Studies for Development of an Updated Photochemical Mechanism for VOC Reactivity Assessment*; California Air Resources Board, Coordinating Research Council, National Renewable Energy Laboratory: 1997.
- (28) Wesely, M. L. *Atmos. Environ.* **1989**, *23*, 1293–1304.
- (29) Maul, P. R. *Atmospheric Transport of Sulfur Compound Pollutants*; Central Electricity Generating Board: Nottingham, England, 1980.
- (30) Hall, G.; Watt, J. M. *Modern Numerical Methods for Ordinary Differential Equations*; Clarendon Press: Oxford, 1976.
- (31) *Midwest Subregional Modeling: Analysis of NOx SIP Call*; Illinois Environmental Protection Agency, Indiana Department of Environmental Management, Michigan Department of Environmental Quality, Wisconsin Department of Natural Resources: Chicago, IL, March, 1999.
- (32) Lyons, W. A.; Tremback, C. J.; Pielke, R. A. *J. Appl. Meteor.* **1995**, *34*, 1762–1784.
- (33) Geron, C. D.; Guenther, A. B.; Pierce, T. E. *J. Geophys. Res.* **1994**, *99*, 12773–12791.
- (34) *User's Guide to MOBILE5*; U.S. Environmental Protection Agency: Ann Arbor, MI, 1994.
- (35) Sandu, A. *Sensitivity Analysis of ODE Via Automatic Differentiation*, MS Thesis, University of Iowa, Iowa City, IA, August, 1997.
- (36) Zhang, Y.; Bischof, C. H.; Easter, R. C.; Wu, P.-T. *J. Geophys. Res.* **1998**, *103*, 18953–18979.

Received for review September 5, 2001. Revised manuscript received April 16, 2002. Accepted April 24, 2002.

ES0112691